

## Exclusive $J/\psi$ and $\Upsilon$ production in high-energy $pp$ and $p$ -Pb collisions

C. A. Flett<sup>1,2</sup>, S. P. Jones<sup>3</sup>, A. D. Martin<sup>3</sup>, M. G. Ryskin<sup>3,\*</sup> and T. Teubner<sup>4</sup>

<sup>1</sup>*Department of Physics, University of Jyväskylä, P.O. Box 35, Jyväskylä 40014, Finland*

<sup>2</sup>*Helsinki Institute of Physics, University of Helsinki, P.O. Box 64, Helsinki 00014, Finland*

<sup>3</sup>*Institute for Particle Physics Phenomenology, Durham University, Durham DH1 3LE, United Kingdom*

<sup>4</sup>*Department of Mathematical Sciences, University of Liverpool, Liverpool L69 3BX, United Kingdom*



(Received 27 June 2022; accepted 19 September 2022; published 20 October 2022)

We present a formalism for determining the cross section for exclusive heavy vector meson production ( $J/\psi$ ,  $\Upsilon$ ) as a function of rapidity, in both high-energy proton-proton and proton-heavy ion collisions, at next-to-leading order in QCD. We compare and contrast the production in  $pp$  and  $p$ -Pb collisions and show how data for these processes can give information on the low- $x$  gluon distribution of the proton and heavy ions at a range of different scales.

DOI: [10.1103/PhysRevD.106.074021](https://doi.org/10.1103/PhysRevD.106.074021)

### I. INTRODUCTION

There is a long history of experimental and theoretical study of exclusive vector meson production in high-energy proton-proton collisions. In particular, data for the differential cross section  $d\sigma(p + p \rightarrow p + V + p)/dY$  have come under theoretical scrutiny for vector mesons  $V = J/\psi, \Upsilon(1S)$ , where the  $+$  signs denote large rapidity gaps between the rapidity  $Y$  of the vector meson and the outgoing protons, ensuring the exclusivity of the experimental measurements. The theoretical description proceeds by first calculating the differential cross section for the exclusive photoproduction subprocess  $\gamma + p \rightarrow V + p$  for which the dominant QCD diagram is sketched in simplified form in Fig. 1. At high energy the process is driven by the behavior of the gluon parton distribution of the proton at small momentum fraction. In this work, we apply the theoretical framework, based on collinear factorization and developed to next-to-leading order (NLO) in perturbative QCD in Refs. [1,2], to  $p$ -Pb collisions. Other approaches include, for example, models based on the color-glass-condensate (CGC) [3,4] and  $k_T$ -factorization frameworks [5], as well as LO perturbative QCD [6]. Note that the two exchanged gluons in Fig. 1 carry different fractions of the incoming proton momentum, so we are dealing with a generalized, skewed gluon distribution. The net momentum fraction transferred from the proton to the

vector meson is  $2\xi$ ; thus, for this exclusive process  $2\xi$  plays the role of the usual variable “ $x$ ” in deep inelastic scattering (DIS). For our high-energy process we have  $x - \xi \ll x + \xi \ll 1$  and the cross section can be accurately estimated in terms of the conventional gluon distribution  $g(2\xi)$  and a skewing correction [7,8]. Recall that a detailed NLO analysis of the current inclusive data determines the NLO gluon distribution down to  $2\xi \simeq 10^{-4}$  [9]. For smaller momentum fractions the uncertainties become too large; see also [10]. However, the exclusive  $J/\psi$  data from LHC [11,12] are found to determine the gluon distribution down to  $2\xi \sim 3 \times 10^{-6}$ .

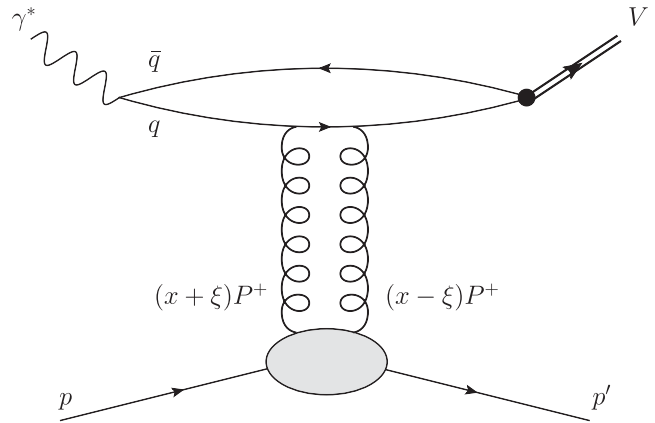


FIG. 1. A schematic diagram of high-energy exclusive vector meson production,  $\gamma^* + p \rightarrow V + p$ . The factorized form follows since, in the proton rest frame, the formation time  $\tau_f \simeq 2E_\gamma/(Q^2 + M_V^2)$  is much greater than the  $q\bar{q}$ -proton interaction time.  $Q$  is the virtuality of the photon and the light-cone momentum  $P^+ = (p + p')/2$ . For the photoproduction setup considered here, we have  $Q^2 = 0$ .

\*Also at Petersburg Nuclear Physics Institute, NRC Kurchatov Institute, Gatchina, St. Petersburg, 188300, Russia.

Published by the American Physical Society under the terms of the [Creative Commons Attribution 4.0 International license](https://creativecommons.org/licenses/by/4.0/). Further distribution of this work must maintain attribution to the author(s) and the published article's title, journal citation, and DOI. Funded by SCOAP<sup>3</sup>.

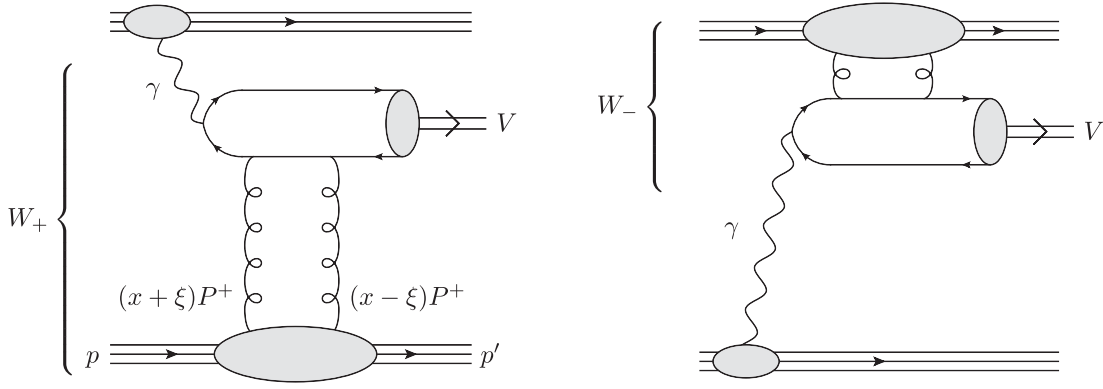


FIG. 2. The two diagrams describing exclusive heavy vector meson production in  $p + p \rightarrow p + V + p$ , at the LHC. The  $W_+$  and  $W_-$  contributions arise in the ultraperipheral description of the  $\gamma + p \rightarrow V + p$  subprocess; see the text for details. In the  $p$ -Pb mode, either the upper or lower proton is replaced by a Pb ion.

In Sec. II we note that in going from the cross section for photoproduction,  $\gamma + p \rightarrow V + p$ , to that for  $p + p \rightarrow p + V + p$ , we need to allow for photon emissions from both incoming protons. Moreover, we have to evaluate the photon flux and the survival factors of the rapidity gaps, i.e. the probabilities that the rapidity gaps do not get populated by additional emissions. Section III concerns exclusive vector meson production in  $p$ -Pb collisions. Data for such a process appear to have the advantage of having a much larger cross section—enhanced by the large charge of the heavy Pb ion, that is, by a factor  $Z^2 = 6724$ . However, when we come to evaluate the cross section we find the theoretical formalism is much more complicated than that for  $pp$  collisions. In Sec. IV we compare the differential cross section data from ALICE and CMS at the proton-nucleon collision energy  $\sqrt{s_{pN}} = 5.02$  TeV for the process  $p + Pb \rightarrow p + V + Pb$ , where  $V = J/\psi, \Upsilon$ , with our corresponding theoretical results. We then provide predictions at  $\sqrt{s_{pN}} = 8.16$  TeV, before presenting our conclusions and outlook in Sec. V.

## II. EXCLUSIVE $p + p \rightarrow p + V + p$ PRODUCTION

We begin with  $pp$  collisions and leave the discussion of  $p$ -Pb collisions until the next section. The procedure for calculating the cross section for the high-energy exclusive process  $p + p \rightarrow p + V + p$  (where the vector meson  $V = J/\psi$  or  $\Upsilon$  and where the  $+$  signs represent rapidity gaps) is described in Refs. [5,13]. As mentioned above, we first calculate the cross section for the exclusive photoproduction process

$$\sigma_W(\gamma p) \equiv \sigma(\gamma + p \rightarrow V + p), \quad (1)$$

where  $W$  is the  $\gamma p$  center-of-mass energy. This process is driven by the two amplitudes sketched in Fig. 2. In the left diagram the photon is radiated by the upper proton and then the vector meson  $V$  is created on the lower proton via the

$\gamma + p \rightarrow V + p$  reaction. The diagram on the right shows the other possibility where the photon is emitted from the lower proton while the upper proton acts as the target.

When the meson  $V$  is detected in the forward region, the corresponding  $\gamma p$  energies are quite different:

$$W_+^2 = M_V \sqrt{s} e^Y \quad \text{and} \quad W_-^2 = M_V \sqrt{s} e^{-Y}, \quad (2)$$

where  $Y$  is the rapidity of the vector meson in the laboratory (i.e.  $pp$  center-of-momentum) frame. Since the  $\gamma p \rightarrow V + p$  cross section steeply grows with energy, the dominant contribution comes from the first amplitude which corresponds to a larger energy  $W_+$ .

The cross section for exclusive  $V$  production in ultraperipheral  $pp$  collisions is therefore given by the sum<sup>1</sup> of the exclusive photoproduction cross sections,  $\sigma_{\pm}(\gamma p)$  of Eq. (1), at the two  $\gamma p$  energies  $W_{\pm}$ :

$$\begin{aligned} \frac{d\sigma(p + p \rightarrow p + V + p)}{dY} = & S^2(W_+) \left( k_+ \frac{dn_p}{dk_+} \right) \sigma_+(\gamma p) \\ & + S^2(W_-) \left( k_- \frac{dn_p}{dk_-} \right) \sigma_-(\gamma p). \end{aligned} \quad (3)$$

Note that the subprocess cross sections are weighted by the survival factors  $S^2(W_{\pm})$ , which account for the probability that the rapidity gap between the vector meson and the target proton is not populated by soft interactions which would destroy the exclusivity of the event, and by the photon fluxes  $dn_p/dk_{\pm}$  for photons of energy  $k_{\pm} = x_{\pm} \sqrt{s}/2$ , where  $x_{\pm}$  are the fractions of the parent proton energy carried by the photon.

The flux of photons emitted from a proton is well known [14]:

<sup>1</sup>The interference between the two amplitudes of the two subprocesses is small since the transverse momentum of the proton which radiates the photon is much smaller than that of the target proton. Thus we may neglect the interference term at the accuracy we are aiming at here.

$$\frac{dn_p(x)}{dx} = \frac{\alpha^{\text{QED}}}{\pi^2 x} \int \frac{d^2 q_\perp}{q_\perp^2 + x^2 m_p^2} \left( \frac{q_\perp^2}{q_\perp^2 + x^2 m_p^2} (1-x) F_E(Q^2) + \frac{x^2}{2} F_M(Q^2) \right), \quad (4)$$

where  $q_\perp$  is the photon transverse momentum,  $m_p$  is the proton mass and  $F_{E,M}$  are the proton form factors:

$$F_E(Q^2) = (4m_p^2 G_E^2(Q^2) + Q^2 G_M^2(Q^2)) / (4m_p^2 + Q^2), \quad (5)$$

$$F_M(Q^2) = G_M^2(Q^2). \quad (6)$$

The scale  $Q^2 = (q_\perp^2 + x^2 m_p^2) / (1-x)$ , while  $G_E$  and  $G_M$  are the ‘‘Sachs’’ form factors, which may be expressed in dipole forms

$$G_E(Q^2) = 1 / (1 + Q^2 / 0.71 \text{ GeV}^2)^2, \quad (7)$$

$$G_M(Q^2) = 2.79 / (1 + Q^2 / 0.71 \text{ GeV}^2)^2. \quad (8)$$

The rapidity gap survival factors  $S^2(W_\pm)$  are calculated in impact parameter  $b$  space using

$$S^2(W_\pm, b) = \exp(-\Omega(b, W_\pm)), \quad (9)$$

where  $\Omega(b, W)$  is the opacity (i.e. optical density) of the proton-proton interaction at the energy  $W$  and the vector valued impact parameter  $\mathbf{b} = (b_x, b_y)$ ; see e.g. [15].

The results as a function of the rapidity of the vector meson are tabulated for different collider energies in Refs. [5,13] for  $V = J/\psi$  and  $\Upsilon$ , respectively.

### III. EXCLUSIVE $p + \text{Pb} \rightarrow p + V + \text{Pb}$ PRODUCTION

In a proton-lead collision the photon flux radiated coherently by the lead ion is strongly enhanced by the factor  $Z^2 = 6724$ . So, as mentioned before, at first sight the amplitude with the photon emitted by the lead ion (say, Fig. 2 left) should dominate. However the situation is not so simple.

#### A. The different contributions

Firstly, in the  $\gamma + \text{Pb} \rightarrow V + \text{Pb}$  process, the nucleons situated at the same impact parameter (i.e. on the line directed along the beam) may interact coherently as well. That is, we have a competition between the factor  $Z^2 = 6724$  and a coherent factor of about  $A^{4/3} = 1232$ ; see [16] for more details. Thus the proton-induced rate is suppressed only by a factor of 5 relative to that induced by Pb.

Moreover, as it is seen from the right-hand side of (4), we have essentially a logarithmic integral  $\int dq_\perp^2 / q_\perp^2$  in the interval from  $q_\perp \simeq xm_p$  up to the value  $\sim 1/R$  limited by the form factors. That is, within the leading-logarithmic approximation, the photon flux is proportional to  $\ln(1/(xm_p R))$ ,

where  $x_\pm = (M_V / \sqrt{s}) e^{\pm Y}$  is the proton momentum fraction carried by the photon and  $R$  is the radius of the photon emitter. Thus, for a large rapidity  $Y$ , the flux radiated by the proton may be enhanced by the ratio

$$\ln(1/(x_- m_p R_p)) / \ln(1/(x_+ m_p R_{\text{Pb}})), \quad (10)$$

which for an  $\Upsilon$  at  $Y = 2.5$  reaches 6.8 at  $\sqrt{s} = 14$  TeV. Here  $(xm_p)^2$  is the minimal virtuality squared,  $|t_{\min}|$ , of the photon which carries the fraction  $x$  of the momentum of the parent proton. The crucial point is that to produce a heavy  $\Upsilon$  at large  $Y$  the photon must carry a large fraction of the nucleon beam momentum and the value of  $xm_p$  becomes comparable to the inverse ion radius,  $1/R_{\text{Pb}}$ . That is, the logarithm in the denominator of the ratio becomes small.

Besides this, the amplitude where the photon was radiated by the proton may be enhanced due to the energy dependence of the elementary photoproduction amplitude.

Therefore, it is not evident that it is sufficient to consider only the photons radiated by the heavy ion. In particular, for the case of forward exclusive  $\Upsilon$  production in the lead ion direction, the contribution caused by the photon radiated off the proton beam may even dominate at large  $Y$ . In our computations we will keep both amplitudes. The kinematic configurations are illustrated (see Fig. 9) and discussed in Appendix B.

#### B. Including the probability of rapidity gap survival

Here we recall the structure of the calculations needed to account for the gap survival probability in *exclusive* vector meson production in  $p$ -Pb collisions. We will follow Sec. VI of Ref. [16]; see also [17].

It is convenient to work in terms of the transverse coordinate, that is, to work in the two-dimensional impact parameter  $b$  space. Let us start with the incoherent production of the vector meson in proton-ion collisions in which the photon is emitted from the incoming proton. The situation is sketched in Fig. 3(a). The figure shows the impact factors  $\mathbf{b}_{\text{Pb}}$ ,  $\mathbf{b}_p$  and  $\mathbf{b}_V$  corresponding, respectively, to the center of the Pb ion, the proton and the produced vector meson. Note that we show the extent in  $b$  space of the Pb ion. It is convenient to take the center of the Pb ion to be the origin of the transverse plane, that is, to take  $\mathbf{b}_{\text{Pb}} = \mathbf{0}$ .

Since we are looking for the cross section ( $\sigma \propto \mathcal{A}^* \mathcal{A}$ ) integrated over the momentum transferred  $t$ , the values of  $b$  are the same in the  $\mathcal{A}^*$  and  $\mathcal{A}$  amplitudes. Allowing for the photon flux and survival factors, we can therefore write the expression for the cross section of the *incoherent*  $p + \text{Pb} \rightarrow p + V + \text{Pb}$  interaction (for the case of the photon radiated by the incoming proton) as

$$\sigma_{\text{incoh}} = \int d^2 b_p d^2 b_V T(b_V) \frac{x dn_p(x, b_p)}{dx} |\mathcal{A}|^2 S_p^2(b_s) S_V^2(b_{sv}), \quad (11)$$

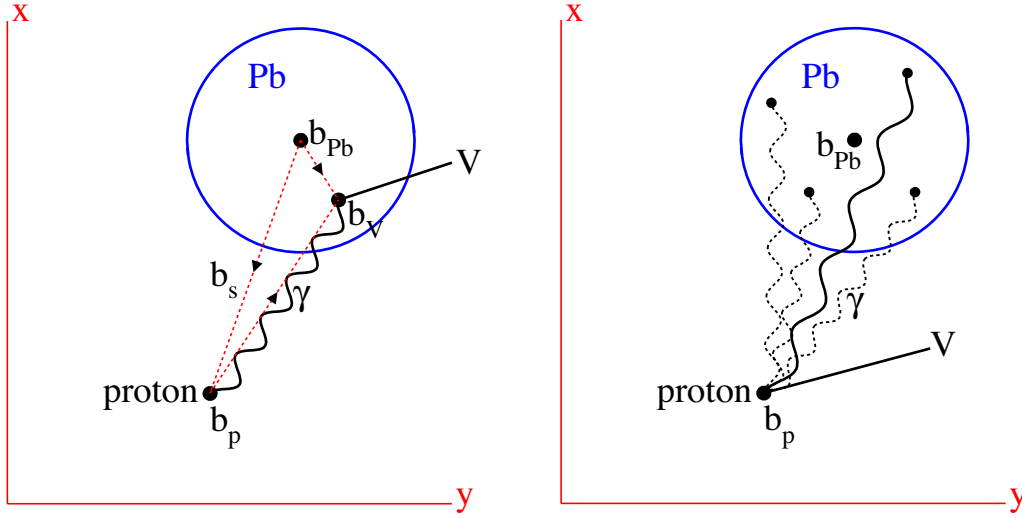


FIG. 3. The geometry of the  $p + \text{Pb} \rightarrow p + V + \text{Pb}$  process in the transverse  $(x, y)$  plane. In the left diagram the photon is radiated off the incoming proton, whereas in the right diagram the photons are radiated by the lead ion. The black dotted curves indicate that we add coherently the contributions of each proton inside the lead ion. Note that the photons can be emitted and absorbed at different points along the  $z$  beam axis.

where  $n_p(x, b)$  is the flux of photons emitted off the proton,  $\mathcal{A} = \mathcal{A}(W, b_a)$  is the  $\gamma + p \rightarrow V + p$  amplitude in  $b$  representation and  $T(b_V)$  is the density profile of the Pb ion, evaluated as given in Appendix A. Equation (11) is written in the limit of a small size amplitude  $\mathcal{A}$ ; i.e. the size of the amplitude given by the  $t$  slope  $B_V = B_0 + 4\alpha' \ln(W/W_0)$  (see later) is much less than that for the heavy ion  $R_{\text{Pb}}^2 \gg 4B_V$ .<sup>2</sup> The survival factors are

$$S_p^2(b_s) = \exp(-T(b_s)\sigma(pN)), \quad (12)$$

which is the probability not to fill the gap by secondary emissions produced in additional proton-lead interactions, where  $b_s = |\mathbf{b}_{\text{Pb}} - \mathbf{b}_p| = b_p$  with our choice  $\mathbf{b}_{\text{Pb}} = \mathbf{0}$ , and

$$S_V^2(b_{sv}) = \exp(-T(b_{sv})\sigma(VN)), \quad (13)$$

which is the probability not to fill the gap by secondaries produced in additional vector meson-Pb interactions, where  $b_{sv} = |\mathbf{b}_{\text{Pb}} - \mathbf{b}_V| = b_V$ . Finally,  $\sigma(pN)$  [and  $\sigma(VN)$ ] are the cross sections of the proton-nucleon (vector meson-nucleon) interaction inside the ion. Recall that the expressions (12) and (13) are similar to the probability not to have

<sup>2</sup>Accounting, however, for the nonlocality of  $\mathcal{A}$  in the computation, i.e. the size of the proton, we replace the density profile  $T(b)$  by the convolution  $T'(b) = \frac{1}{4\pi B_V} \int d^2b' T(b') \exp[-(\mathbf{b} - \mathbf{b}')^2 / (4B_V)]$ . [This is true for any choice of  $b$ . Our natural choice  $T(b_V)$  is given in Eq. (A1).] Analogous replacements (with the corresponding  $B$  slopes) were used in the calculation of the survival factors  $S^2$ . For proton-nucleon interactions the slope  $B_{\text{el}} = 20 \text{ GeV}^{-2}$  is used for  $\sqrt{s_{pN}} = 8.16 \text{ TeV}$  and  $B_{\text{el}} = 19.1 \text{ GeV}^{-2}$  for  $\sqrt{s_{pN}} = 5.02 \text{ TeV}$ .

an additional interaction in the target and the product  $T(b)\sigma$  plays the role of the optical density of the target, that is, the opacity  $\Omega$  in (9).

If we were to neglect the survival factors (i.e. setting  $S^2 = 1$ ), then the cross section would be

$$\sigma_{\text{incoh}} = \frac{xdn_p(x)}{dx} \sigma(\gamma + p \rightarrow V + p) \cdot A, \quad (14)$$

where  $A = 208$  is the lead atomic number.

As mentioned above, besides the incoherent interaction, we need to consider coherent production as well. Here the situation is sketched in Fig. 4. The *coherent* cross section is of the form

$$\sigma_{\text{coh}} = 4\pi B_V F_{\text{Pb}}^2(t_{\min}) \int d^2b_p d^2b_V T^2(b_V) \times \frac{xdn_p(x, b_p)}{dx} |\mathcal{A}|^2 S_p^2(b_s) S_V^2(b_V), \quad (15)$$

where the dimension of the extra  $T$  factor is compensated by the  $t$  slope of the  $\gamma + p \rightarrow V + p$  amplitude.<sup>3</sup> The amplitude  $\mathcal{A}$  is normalized to  $\int d^2b |\mathcal{A}(b)|^2 = \sigma(\gamma + p \rightarrow V + p)$ .

The form factor  $F_{\text{Pb}}$  in (15) accounts for the nucleon distribution in the lead ion. The point is that the coherence of the interaction with different nucleons should not be destroyed by the longitudinal component of the momentum transferred. This component is represented by  $t_{\min} = -(xm_p)^2 / (1-x)$ . Since the value of  $|t_{\min}|$  is small

<sup>3</sup>Recall that the  $t$  behavior of the photoproduction cross section  $d\sigma(\gamma + p \rightarrow V + p)/dt \propto \exp(B_V t)$  corresponds to the amplitude  $\mathcal{A}(b) = \mathcal{A}(b=0) \exp[-b^2 / (2B_V)]$ .

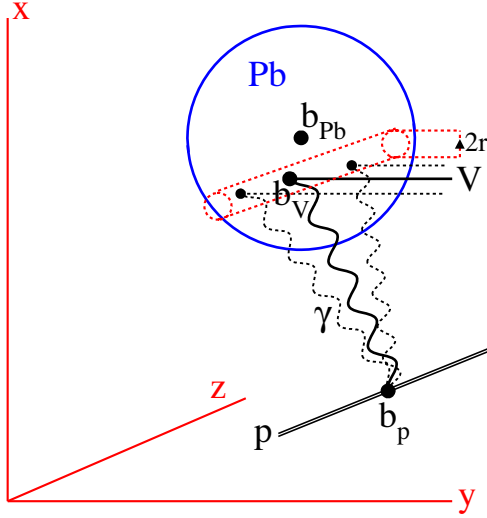


FIG. 4. The geometry of the  $p + \text{Pb} \rightarrow p + V + \text{Pb}$  process, where  $(x, y)$  is the transverse plane and  $z$  is in the direction of the beam. The black dotted curves indicate that we add coherently the contributions of each nucleon absorbing a photon inside the lead ion tube of the radius  $r = \sqrt{4B_V}$  directed along the beam ( $z$ ) axis. The transverse size of the tube,  $r$ , is driven by the  $t$  slope (i.e. the size) of the  $\gamma + N \rightarrow V + N$  amplitude. The extra factor  $4\pi B_V T(b_V)$  in (15) in comparison with (11) is the number of nucleons which may act coherently inside this tube of transverse area  $4\pi B_V$ . Note that the photons can be emitted and absorbed at different points along the  $z$  beam axis, so  $b_V$  covers all the points in the red tube taken appropriately over the Pb ion.

in our kinematics, here we use just the exponential parametrization  $F_{\text{Pb}}(t) = \exp(t\langle r_{\text{Pb}}^2 \rangle / 6)$ , with  $\langle r_{\text{Pb}}^2 \rangle$  being the mean radius squared of the lead ion.

We are particularly interested in the case when the photons are radiated by the lead ion. Then we have only coherent radiation to consider. Here the situation is sketched in the right panel of Fig. 3. Now the cross section has the form

$$\sigma_{\text{Pb}} = \sigma(\gamma + p \rightarrow V + p) \int d^2 b_V \frac{x dn_{\text{Pb}}(x, b_V)}{dx} \times S_p^2(b_V) S_V^2(b_V). \quad (16)$$

Calculating the photon flux  $n(x, b)$  given by (4) we keep just the electric ( $F_E$ ) term since the magnetic ( $F_M$ ) contribution contains an additional  $x^2$  factor, while we work at small  $x$ . Besides this, the magnetic contribution is concentrated at low impact parameters where the gap survival factor  $S_p^2$  is extremely small. [We have checked that the magnetic ( $F_M$ ) contribution does not exceed 1%.] For the lead ion the form factor  $F_E$  corresponds to the proton distribution in lead; see (A2).

Note, however, that expression (4) cannot be transformed to the coordinate  $b$  representation directly. First, we have to transform the *amplitude* of photon emission and to account

for the polarization structure of the amplitude. The point is that the photon polarization vector  $e_\gamma$  is directed parallel to the photon transverse momentum  $\mathbf{q}_\perp$ . That is, the amplitude should be a vector. In  $b$  space it will be the vector  $\mathbf{a}_\gamma = \mathbf{b}a(b)$ . Calculating the Fourier transform gives

$$\mathbf{b}a(b) = \frac{1}{4\pi^2} \int \frac{d^2 q_\perp e^{i\mathbf{b} \cdot \mathbf{q}_\perp}}{(q_\perp^2 + x^2 m_p^2)} \mathbf{q}_\perp \sqrt{\frac{\alpha^{\text{QED}}}{\pi x}} (1-x) F_E(Q^2), \quad (17)$$

and after the angular integration we do not obtain the usual zero-order Bessel  $J_0(\mathbf{b} \cdot \mathbf{q}_\perp)$  but rather  $J_1(\mathbf{b} \cdot \mathbf{q}_\perp)$  [18]. Since  $J_1(\mathbf{b} \cdot \mathbf{q}_\perp)$  vanishes as  $b \rightarrow 0$ , the typical values of the impact parameter become larger.

Finally the photon flux in the  $b$  representation outside the heavy ion takes the form

$$\frac{d^3 n_{\text{Pb}}}{dx d^2 b_\gamma} = \frac{Z^2 \alpha^{\text{QED}}}{x \pi^2 b_\gamma^2} (x m_p b_\gamma)^2 K_1^2(x m_p b_\gamma), \quad (18)$$

where  $K_1(z)$  is the modified Bessel function.

### C. The uncertainty in the evaluation of $S^2$

Note that the expression for  $S_V$  in (13) is written in the spirit of the vector meson dominance model [19,20]. That is, we *assume* that the photon to  $\Upsilon$  transition takes place *before* the collision and then the *completely dressed*  $\Upsilon$  meson interacts with the heavy ion. This is reasonable when the meson goes in the proton beam direction (see [21] for a detailed discussion). However, the assumption is not justified for a very forward (large rapidity)  $\Upsilon$  going in the direction of the lead ion. Indeed, the  $\gamma \rightarrow b\bar{b}$  vertex is pointlike and for  $Y > 2-3$  the quarks do not have sufficient time to form the normal  $\Upsilon$  wave function. From the beginning the size of the  $b\bar{b}$  pair is too small, and the corresponding cross section [22,23]

$$\sigma(VN) \propto \alpha_s^2 \langle r_{b\bar{b}}^2 \rangle \quad (19)$$

is smaller than the cross section of the normally dressed  $\Upsilon$  meson.

In addition, the absorption cross section for the  $\Upsilon$  meson,  $\sigma(VN)$ , is not known experimentally. Moreover it depends on the  $VN$  collision energy  $s_{VN} = W^2$ . For our numerical estimate we take the Regge behavior

$$\sigma_{VN}(W) = \sigma_0 \left( \frac{W^2}{M_V^2} \right)^{\alpha_p(0)-1} \quad (20)$$

and assume that  $\sigma_0 \propto 1/M_V^2$ . The normalization is fixed to the  $J/\psi$  absorptive cross section  $\sigma(J/\psi N) \simeq 4$  mb at

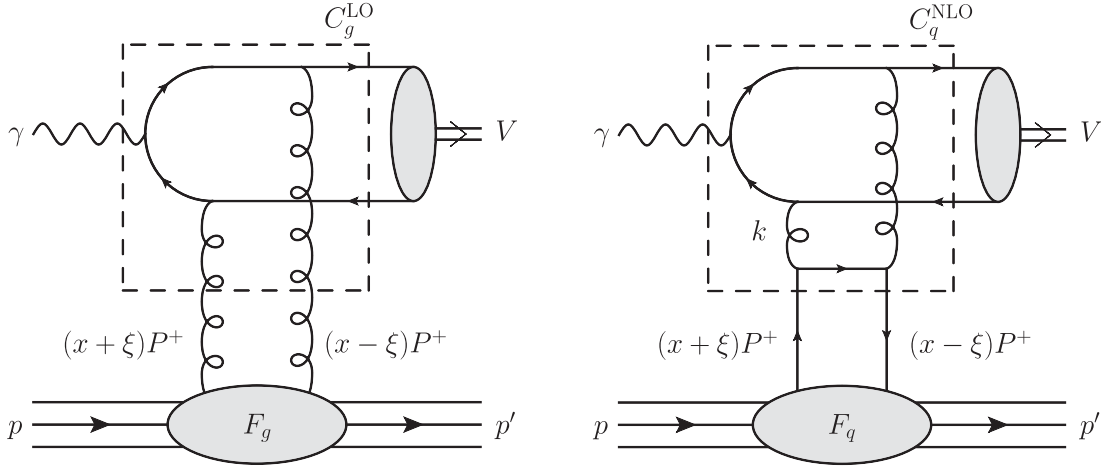


FIG. 5. The LO and the NLO quark contributions to  $\gamma + p \rightarrow V + p$  amplitude. The parton momentum fractions are  $x + \xi$  and  $x - \xi$  and  $k$  is the loop momentum.

$W \simeq 10$  GeV for a completely dressed  $J/\psi$  meson measured by the N50 Collaboration [24]. For the Pomeron intercept we take  $\alpha_p(0) - 1 = 0.25$ . This is consistent with the DIS data and the intercept of the Balitsky-Fadin-Kuraev-Lipatov Pomeron after the resummation of the next-to-leading logarithmic corrections [25–28]. Since the expected value of  $\sigma(\Upsilon N)$  is small, the survival probability due to  $\Upsilon$  absorption,  $S_V^2$ , is rather close to unity.

To demonstrate the effect, we compare the obtained results with those taking  $\sigma(\Upsilon N) = 0$ . The difference never exceeds 6%–10%. Accounting for the “undressed meson” problem this means that for the mesons going with large rapidity in the lead ion direction the true value of  $S^2$  may be about 3%–5% larger.

Finally, there is some uncertainty due to the value of the proton-nucleon cross section  $\sigma(pN)$ . Recall that at 8 TeV TOTEM had measured  $\sigma_{\text{tot}}(pp) = (103 \pm 2.3)$  mb [29], while ATLAS-ALFA gives  $(96 \pm 1)$  mb [30]. Here we take  $\sigma(pN) = 100$  mb for our numerics. The corresponding uncertainty is about 3%–4%.

#### D. Numerical results for (photon flux) $\times$ (gapon survival)

For proton-lead collisions, Eq. (3) is replaced by the form

$$\begin{aligned} & \frac{d\sigma(p + \text{Pb} \rightarrow p + V + \text{Pb})}{dY} \\ &= S^2(W_{\text{Pb}}) \left( k_+ \frac{dn_{\text{Pb}}}{dk_+} \right) \sigma_{\gamma p}(W_{\text{Pb}}) \\ &+ S^2(W_p) \left( k_- \frac{dn_p}{dk_-} \right) (\sigma_{\text{incoh}}(W_p) + \sigma_{\text{coh}}(W_p)) R_A^2, \quad (21) \end{aligned}$$

where the nuclear modification factor  $R_A(2\xi) = g_{\text{Pb}}(2\xi)/g_p(2\xi)$  accounts for the fact that the gluon

distribution<sup>4</sup> in the lead ion may differ from the sum of the gluon distributions in free nucleons. The value of the nucleon modification factor  $R_A(2\xi)$  at the corresponding scale  $\mu = M_V/2$  is taken from the EPPS16 NLO analysis [31]. It is convenient to introduce the so-called “effective fluxes”  $f_{\text{Pb}}$  and  $f_p$ , which include the original photon flux  $x dn/dx$  times the survival and nuclear modification effects.<sup>5</sup> The effective flux radiated by the lead ion is

$$f_{\text{Pb}}(2\xi) = \frac{\sigma_{\text{Pb}}}{\sigma(\gamma + p \rightarrow V + p)}, \quad (22)$$

where  $\sigma_{\text{Pb}}$  is given by (16). The effect of the flux radiated by the proton is given by the sum of coherent and incoherent fluxes

$$f_{\text{incoh}}(2\xi) = \frac{\sigma_{\text{incoh}}}{\sigma(\gamma + p \rightarrow V + p)} R_A^2(2\xi) \quad (23)$$

and

$$f_{\text{coh}}(2\xi) = \frac{\sigma_{\text{coh}}}{\sigma(\gamma + p \rightarrow V + p)} R_A^2(2\xi), \quad (24)$$

where  $\sigma_{\text{incoh}}$  and  $\sigma_{\text{coh}}$  are given by (11) and (15), respectively. Here,  $2\xi = 2M_V^2/(2W^2 - M_V^2) \approx M_V^2/W^2$  for  $W^2 \gg M_V^2$ , i.e.  $2\xi \ll 1$ , is the fractional momentum transfer provided by the two-gluon exchange.

Finally, the cross section of heavy vector meson production can be written as

<sup>4</sup>Recall that the value of  $\sigma(\gamma + p \rightarrow V + p) \propto (2\xi g(2\xi))^2$  is almost completely driven by the gluon distribution.

<sup>5</sup>It is not completely correct to use the word “flux” for a quantity which includes these additional effects; however, we use it since it enables us to shorten the description of the computations.

$$\begin{aligned} & \frac{d\sigma(p + \text{Pb} \rightarrow p + V + \text{Pb})}{dY} \\ &= f_{\text{Pb}}(W_{\text{Pb}})\sigma_{\gamma p}(W_{\text{Pb}}) + (f_{\text{incoh}}(W_p) \\ & \quad + f_{\text{coh}}(W_p))\sigma_{\gamma p}(W_p). \end{aligned} \quad (25)$$

Here the values of  $W_{\text{Pb}}$  and  $W_p$  correspond to the energies of the  $\gamma + p \rightarrow V + p$  process initiated by the photon emitted off the lead ion and proton beam, respectively.

The values of the effective fluxes are presented in Tables I and II in Appendix B for  $\Upsilon$  and  $J/\psi$  production at proton-nucleon collision energy  $\sqrt{s_{pN}} = 5.02$  TeV. The analogous values at  $\sqrt{s_{pN}} = 8.16$  TeV are given in Tables III and IV.

#### IV. COMPARISON WITH DATA

In this section, we compare our theoretical predictions with the rapidity differential cross section data from ALICE [32,33] and CMS [34] for the process  $p + \text{Pb} \rightarrow p + V + \text{Pb}$ , where  $V = J/\psi, \Upsilon$ . Using Eq. (25) we compute  $d\sigma(p + \text{Pb} \rightarrow p + J/\psi + \text{Pb})/dY$ , with  $\sigma_{\gamma p}$  evaluated using, as input, the gluon parton distribution function (PDF) fit obtained from our previous analyses [35].

We work at NLO within the collinear factorization scheme and express the amplitude for exclusive heavy vector meson photoproduction as

$$\begin{aligned} \mathcal{A} &= \frac{4\pi\sqrt{4\pi}\alpha_e(\epsilon_V^* \cdot \epsilon_\gamma)}{N_c} \left( \frac{8\langle O_1 \rangle_V}{M_V^3} \right)^{1/2} \\ & \times \int_{-1}^1 dx (C_g(x, \xi)F_g(x, \xi) + C_q(x, \xi)F_q(x, \xi)), \end{aligned} \quad (26)$$

where  $F_g$  and  $F_q$  are the gluon and quark singlet generalized parton distributions,  $C_g$  and  $C_q$  are the gluon and quark coefficient functions, respectively (see [1,2]), and  $x - \xi, x + \xi$  are the parton momentum fractions in the light-cone direction  $P^+$ . The corresponding gluon and quark coefficient functions for exclusive heavy vector meson electroproduction were calculated in Refs. [36,37]. The dependence on the factorization and renormalization scales  $\mu_F$  and  $\mu_R$ , respectively, and on the four-momentum transfer squared,  $t$ , is not shown. The setup is illustrated in Fig. 5. The nonrelativistic QCD matrix element  $\langle O_1 \rangle_V$  is fixed by the experimental value of the heavy vector meson decay width to a dilepton pair; see [38].

We take  $\mu_R = \mu_F$  and use the ‘‘optimal’’ factorization scale  $\mu_F = M_V/2$ ; see [39]. That is, the exclusive  $J/\psi$  and  $\Upsilon$  photoproduction data probe the gluon densities at two different scales. Besides this, we implement the  $Q_0$  subtraction [2] needed to avoid the double counting between the low  $k_T < Q_0$  contributions in the NLO coefficient functions and that hidden in the PDF inputs.

This choice provides a sufficiently good scale stability of the prediction.<sup>6</sup>

The cross section  $\sigma_{\gamma p}$ , integrated over the Mandelstam variable  $t$ , is given by

$$\begin{aligned} \sigma_{\gamma p}(W) &= \frac{1}{B_V(W)} \left( \frac{d\sigma}{dt}(\gamma p \rightarrow V p) \Big|_{t=0} \right) \\ &= \frac{1}{B_V(W)} \frac{(\text{Im}\mathcal{A})^2(1 + \rho^2)}{16\pi W^4}, \end{aligned} \quad (27)$$

where

$$\rho = \frac{\text{Re}\mathcal{A}}{\text{Im}\mathcal{A}} = \tan \left( \frac{\pi}{2} \frac{\partial \ln(\text{Im}\mathcal{A}/W^2)}{\partial \ln W^2} \right) \quad (28)$$

is the real part correction (see e.g. [40]) and  $B_V(W)$  is the Regge-motivated energy-dependent slope parameter given by

$$B_V(W) = \left( B_0 + 4\alpha'_p \ln \left( \frac{W}{W_0} \right) \right) \text{GeV}^{-2}. \quad (29)$$

Here,  $B_0 = 4.9$  for  $V = J/\psi$  [41] and  $B_0 = 4.63$  for  $V = \Upsilon$ , with  $\alpha'_p = 0.06$  and  $W_0 = 90$  GeV [42]. The smaller value of  $B_0$  for the case  $V = \Upsilon$  is due to the need for reducing the  $J/\psi$  slope parameter by the factor  $4\alpha' \ln(M_\Upsilon/M_{J/\psi})$ .

Figure 6 shows our rapidity differential cross section predictions at  $\sqrt{s_{pN}} = 5.02$  TeV for the process  $p + \text{Pb} \rightarrow p + V + \text{Pb}$ . The upper row shows the predictions for  $V = J/\psi$  and the lower one for  $V = \Upsilon$ . In the left panels, we show the decomposition of the total cross section result into the  $\gamma p$  contribution [the first term on the right-hand side of Eq. (25), labeled by  $\sigma_{\text{Pb}}$  in the figure] and the  $\gamma$ -Pb contribution [the second term on the right-hand side of Eq. (25), labeled by  $\sigma_p$  in the figure]. In the right panels, we show our results compared with existing data from ALICE and/or CMS [32–34]. The error bands are indicative of the uncertainty due to our previous low- $x$  gluon PDF fit [35] only and does not account for theoretical uncertainties in the present formalism. We emphasize that no fit is performed to the  $p$ -Pb data here, and the width of the bands is given by propagating the errors on the fit parameters using the full covariance matrix obtained from our previous gluon PDF fit made to the low- $x$  exclusive  $J/\psi$  data in  $pp$  collisions in Ref. [35].

For  $V = J/\psi$ , the  $\gamma$ -Pb contribution is less than a percent at midrapidity, while for  $V = \Upsilon$ , it is as much as 7%. The mass of the  $\Upsilon$  is  $\sim 3$  times that of the  $J/\psi$  and so (with  $k_+ \propto M_V$  and  $W_+ \propto \sqrt{M_V}$ ) the typical photon energy in exclusive  $\Upsilon$  production is now much larger than in exclusive  $J/\psi$  production for a given  $Y_{\text{lab}}$ . Therefore,

<sup>6</sup>Recall that exactly the same approach (that is, use of the optimal scale  $\mu_F = M_V/2$  and the  $Q_0$  subtraction) was applied in Ref. [35] to determine the low- $x$  gluon PDF from exclusive  $J/\psi$  data, used in the present analysis.

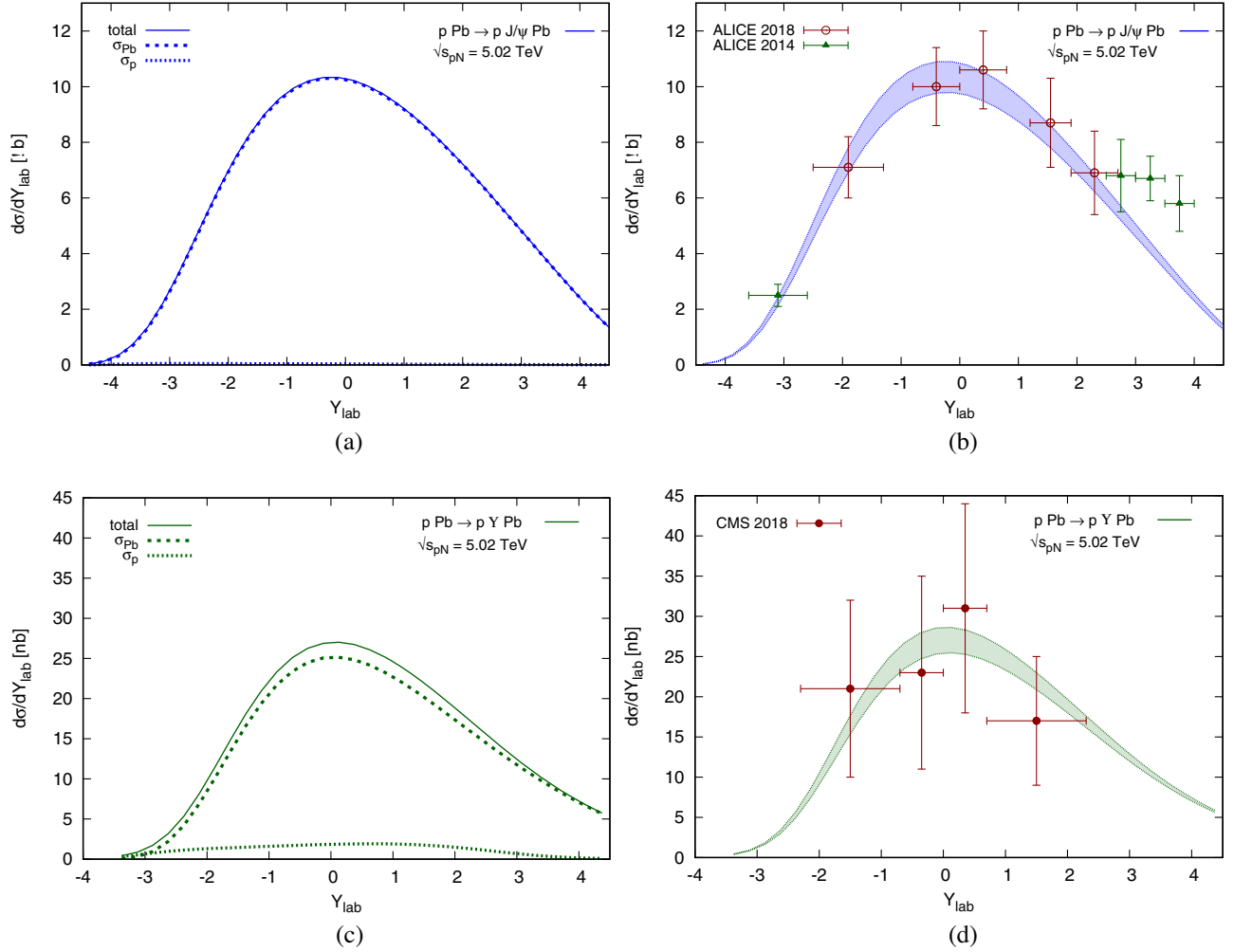


FIG. 6. Theoretical predictions for coherent exclusive  $J/\psi$  and  $Y$  photoproduction rapidity differential cross sections in  $p$ -Pb collisions with  $\sqrt{s_{pN}} = 5.02$  TeV. Panels (a) and (c) show the decomposition of the total cross section into the  $\sigma_{Pb}$  and  $\sigma_p$  contributions; see text for details. Panels (b) and (d) compare our predictions with existing data from ALICE and/or CMS [32–34]. We emphasize that no fit is made to the data shown; the width of the uncertainty bands is obtained by the  $\pm 1\sigma$  statistical uncertainties and the normalization errors of the datasets used in our previous fit [35] to determine the low- $x$  gluon PDF, which is used in the present analysis.

the photon flux radiated off Pb is relatively suppressed for  $Y$  production. We remark that for  $Y_{lab} < -3$  in Fig. 6(c), the photon radiated by Pb has a somewhat greater  $x$  (with respect to the nucleon in Pb) and so the value of  $b_V = b_\gamma$  [in Eq. (18)] is rather small. This means that the integrated flux from Pb is not large and  $S^2(b_V)$  is small. On the other hand, the photon radiated by the proton has a much smaller  $x$  (with respect to the proton) leading to a larger  $S^2$  and a larger integrated flux. This is evident from Table III where, for  $Y_{lab} < -3$ , the value of  $f_{Pb}$  is an order of magnitude smaller than  $f_p$ . The energy dependence of  $\sigma(\gamma + N \rightarrow V + N)$  does not compensate this difference for  $\sqrt{s_{pN}} = 5.02$  TeV. This accounts for the  $W_p$  contribution being greater than the  $W_{Pb}$  one in this region.

Our predictions agree favorably with the ALICE data, particularly at backward, central and semiforward rapidities.

For  $V = J/\psi$ , our prediction undershoots the data for  $Y_{lab} \geq 2.5$ . In this region, however, our prediction is well constrained. As shown above, the dominant contribution comes from the photon radiated by Pb, occurring at large  $b$ , with  $S^2$  very close to unity where we have practically no uncertainty in the photon flux. On the other hand, the “gamma-proton” center-of-mass energy is relatively small, and this is precisely the region where our gluon PDF fit agreed well with the HERA data [35]. The earlier ALICE data from Ref. [32] for  $Y_{lab} \geq 2.5$  show an unexpected plateauing behavior and are arguably inconsistent with those in Ref. [33].<sup>7</sup>

<sup>7</sup>The behavior of the earlier ALICE data in Fig. 6(b) are incompatible with other theoretical predictions, too; see e.g. Fig. 4 of Ref. [6].

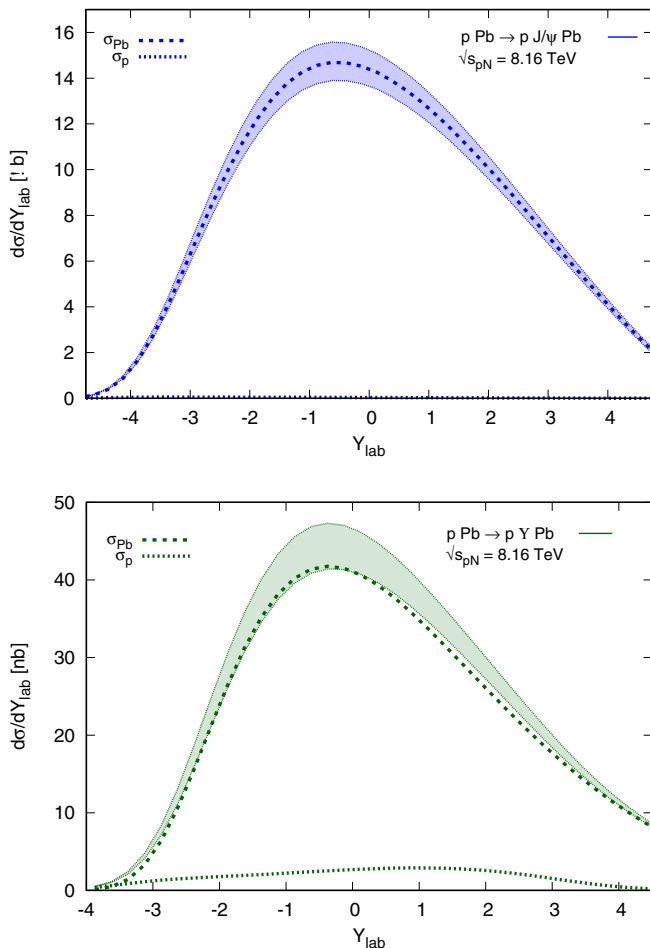


FIG. 7. Theoretical predictions for coherent exclusive  $J/\psi$  and  $\Upsilon$  photoproduction rapidity differential cross sections in  $p$ -Pb collisions with  $\sqrt{s_{pN}} = 8.16$  TeV. The bands and curves are as described in the caption of Fig. 6. Note that currently there are no data for the process  $p + \text{Pb} \rightarrow p + V + \text{Pb}$ , with  $V = J/\psi, \Upsilon$ , at this center-of-mass energy, but measurements for  $\Upsilon$  photoproduction are shortly anticipated [43,44].

In Fig. 7, we show the analogous set of plots at  $\sqrt{s_{pN}} = 8.16$  TeV. There are currently no data for  $p + \text{Pb} \rightarrow p + V + \text{Pb}$  at this center-of-mass energy, but forthcoming measurements for the case  $V = \Upsilon$  from CMS are anticipated [43,44]. Our results for the rapidity distribution are qualitatively consistent with the shapes predicted by other approaches; however, the normalization of our prediction is larger than that obtained from CGC models [3,4].

In both Figs. 6 and 7, note that the larger  $d\sigma/dY_{\text{lab}}$  at positive  $Y_{\text{lab}}$  is indicative of the proton direction corresponding to the positive  $Y_{\text{lab}}$ . At negative  $Y_{\text{lab}}$  the distribution is skewed due to a smaller energy per nucleon in the Pb ion. Indeed, at large rapidities in the Pb direction (i.e. large negative  $Y_{\text{lab}}$ ), the contribution due to the photon radiated from Pb is strongly suppressed, especially in the  $\Upsilon$  case, since the momentum fraction  $x \propto (M_V/\sqrt{s}) \exp(Y)$

carried by the photon becomes large and the transverse momentum cutoff  $xm_p$  becomes comparable with the inverse lead ion radius  $1/R_{\text{Pb}}$ ; i.e. here we deal with the impact parameter  $b_V \sim R_{\text{Pb}}$ . Therefore, in this region, the survival factor  $S^2(b_V)$  suppresses the  $\sigma_{\text{Pb}}$  contribution, and the second term of (25), i.e. the photons radiated by the proton, starts to dominate.

## V. CONCLUSIONS

We have predicted the cross sections for exclusive  $J/\psi$  and  $\Upsilon$  meson production in proton-lead ion collisions at the LHC for center-of-mass energies  $\sqrt{s_{pN}} = 5.02$  TeV and  $\sqrt{s_{pN}} = 8.16$  TeV, using the low- $x$  gluon distribution extracted in Ref. [35] from the data on  $p + p \rightarrow p + J/\psi + p$ . We account for the gap survival probability caused by both the additional proton-lead interactions and the interaction of the secondary vector meson inside the heavy ion.

As expected, the dominant contribution to the cross section in exclusive  $p$ -Pb collisions comes from the amplitude where the photon is radiated by the lead ion (for all rapidities  $Y_{\text{lab}} \gtrsim -3$ ). However, our detailed study finds that the naively expected dominance of the  $Z^2$  enhancement of the cross section, when we go from exclusive production from photons radiated by a proton to that for photons radiated by the heavy ion, is considerably reduced. Nevertheless, we find that the enhancement is still sufficient to enable forthcoming data for exclusive heavy vector meson production in  $p$ -Pb collisions to provide additional constraints on the *free* proton gluon PDF at low to moderate values of  $x$  and scale. Such data could be used in a combined fit with those in  $pp$  collisions anticipated from the high-luminosity phase of the LHC, as well as in the upcoming  $ep$  program of the electron-ion collider, to provide refined constraints on the gluon PDF.

## ACKNOWLEDGMENTS

We thank Petja Paakinen for providing the numerical values for the EPPS16 gluon modification factor at the scales  $\mu^2 = m_c^2$  and  $\mu^2 = m_b^2$  used in this work. C. A. F. is supported by the Helsinki Institute of Physics core funding Project No. QCD-THEORY. S. P. J. is supported by a Royal Society University Research Fellowship (Grant No. URF/R1/201268). The work of T. T. is supported by the STFC Consolidated Grant No. ST/T000988/1. This work is also supported in part by the STFC Grant No. ST/T001011/1.

## APPENDIX A: DENSITY PROFILE OF THE Pb ION

The density profile of the Pb ion felt by the proton may be written in the form

$$T(b_V) = \int_{-\infty}^{+\infty} dr_z (\rho_p(r) + \rho_n(r)), \quad (\text{A1})$$

where in terms of the transverse vectors  $\mathbf{b}_V$  and  $\mathbf{b}_{\text{Pb}}$ , the impact parameter  $r_t = |\mathbf{b}_V - \mathbf{b}_{\text{Pb}}|$  and with our choice of the origin of the transverse plane,  $\mathbf{b}_{\text{Pb}} = 0$ , we have  $r_t = b_V$  with  $r = \sqrt{r_z^2 + r_t^2}$ . For the nucleon density in lead,  $\rho(r)$ , we use the Woods-Saxon form [45]

$$\rho_N(r) = \frac{\rho_0}{1 + \exp((r - R)/d)}, \quad (\text{A2})$$

where the parameters  $d$  and  $R$ , respectively, characterize the skin thickness and the radius of the nucleon density in the heavy ion;  $\mathbf{r} = (r_z, r_t)$ . For  $^{208}\text{Pb}$  we take the recent results of Refs. [46,47]:

$$\begin{aligned} R_p &= 6.680 \text{ fm}, & d_p &= 0.447 \text{ fm}, \\ R_n &= (6.67 \pm 0.03) \text{ fm}, & d_n &= (0.55 \pm 0.01) \text{ fm}. \end{aligned} \quad (\text{A3})$$

The nucleon densities  $\rho$  are normalized to

$$\int \rho_p(r) d^3r = Z, \quad \int \rho_n(r) d^3r = N_n, \quad (\text{A4})$$

for which the corresponding proton (neutron) densities are  $\rho_0 = 0.063$  ( $0.093$ )  $\text{fm}^{-3}$ .

## APPENDIX B: TABLES OF EFFECTIVE FLUXES

The values of the effective fluxes used in Eq. (25) are presented in Tables I and II below for  $\Upsilon$  and  $J/\psi$  production at proton-nucleon collision energy  $\sqrt{s_{pN}} = 5.02$  TeV. The analogous values at  $\sqrt{s_{pN}} = 8.16$  TeV are also given, in Tables III and IV.

The first column is the rapidity  $Y_{\text{lab}}$  of the vector meson measured in the laboratory frame. We account for the asymmetry of proton-ion collisions. In the case of lead we have (in the laboratory frame) a proton beam momentum

equal to 4 TeV (6.5 TeV), while the momentum of a nucleon in lead is  $4(Z/A) = 1.58$  TeV [ $6.5(Z/A) = 2.56$  TeV] for  $\sqrt{s_{pN}} = 5.02$  (8.16) TeV. Positive  $Y_{\text{lab}} > 0$  corresponds to the vector meson going in the proton direction.

The second and fourth columns are the  $\gamma$ -nucleon collision energies  $W_{\text{Pb}}$  and  $W_p$ , respectively. The effective flux  $f_{\text{Pb}}$  is given in the third column while the fluxes  $f_{\text{incoh}}$  and  $f_{\text{coh}}$  and their sum are shown in the fifth, sixth and seventh column, respectively.

Column eight gives the sum  $f_{\text{incoh}} + f_{\text{coh}}$  for the case  $R_A = 1$ . The factor of  $R_A$  enters only the term where the photon is radiated by the proton and, as shown in Figs. 6 and 7, this contribution is relatively small (especially for  $J/\psi$ ) and can be seen at large backward rapidities only. The contribution due to the term where the photon is radiated from the proton with and without inclusion of the nuclear modification factor,  $R_A$ , is shown in Fig. 8. This difference at the total cross section level amounts to at most a few percent only for the  $J/\psi$  case because the contribution when the photon is radiated from the lead ion dominates. Therefore, the nuclear modification factor is hardly seen in  $p$ -Pb collisions, where the first term of (25) dominates. This factor can be much better observed (and measured) in the Pb-Pb setup; see e.g. [48] for a baseline description of the  $\text{Pb} + \text{Pb} \rightarrow \text{Pb} + J/\psi + \text{Pb}$  process in the collinear factorization framework to NLO.

Note that, in asymmetric  $p$ -Pb collisions, the laboratory frame does not coincide with the center-of-momentum frame of the  $p$ -Pb system and so Eq. (2) should be adjusted. For the case where the vector meson is detected at positive rapidities (corresponding to the configurations in the upper row of Fig. 9),

$$\begin{aligned} W_+^2 &= M_V \sqrt{s} e^{+(Y_{\text{lab}} - Y_0)} = W_p^2 \quad \text{and} \\ W_-^2 &= M_V \sqrt{s} e^{-(Y_{\text{lab}} - Y_0)} = W_{\text{Pb}}^2, \end{aligned} \quad (\text{B1})$$

where  $Y_0 = 0.465$  is the shift of the nucleon-nucleon center of mass with respect to the laboratory frame.

TABLE I. The effective photon flux  $f_{\text{Pb}}$  and  $f_{\text{incoh}}$ ,  $f_{\text{coh}}$  radiated in the case of  $\Upsilon$  production at proton-nucleon collision energy  $\sqrt{s_{pN}} = 5.02$  TeV by the lead ion and by the proton beam.

$Y_{\text{lab}}$	$W_{\text{Pb}}$ (GeV)	$f_{\text{Pb}}$	$W_p$ (GeV)	$f_{\text{incoh}}$	$f_{\text{coh}}$	$f_{\text{incoh}} + f_{\text{coh}}$	$f_{\text{incoh}} + f_{\text{coh}}(R_A = 1)$
-5.125	3570	$0.464 \times 10^{-12}$	13.31	6.23	0.0	6.23	7.16
-4.875	3150	$0.577 \times 10^{-10}$	15.08	5.77	$0.52 \times 10^{-21}$	5.77	6.91
-4.625	2780	$0.930 \times 10^{-8}$	17.09	6.37	$0.22 \times 10^{-10}$	6.37	6.66
-4.375	2450	$0.725 \times 10^{-6}$	19.37	6.83	$0.51 \times 10^{-5}$	6.83	6.41
-4.125	2160	$0.262 \times 10^{-4}$	21.95	7.11	$0.39 \times 10^{-2}$	7.11	6.16
-3.875	1910	$0.481 \times 10^{-3}$	24.87	7.21	0.15	7.36	6.03
-3.625	1690	$0.500 \times 10^{-2}$	28.18	7.17	1.2	8.35	6.60
-3.375	1490	$0.326 \times 10^{-1}$	31.93	7.03	3.9	10.9	8.38
-3.125	1310	0.146	36.18	6.75	7.5	14.2	10.9
-2.875	1160	0.482	41.00	6.29	11	16.8	13.2
-2.625	1020	1.26	46.46	5.64	12	17.8	14.7
-2.375	902	2.71	52.64	4.97	12	17.4	15.5
-2.125	796	5.03	59.65	4.36	12	16.3	15.6
-1.875	703	8.33	67.60	3.81	11	14.9	15.4
-1.625	620	12.6	76.60	3.35	10	13.4	14.8
-1.375	547	17.7	86.80	2.96	9.1	12.1	14.1
-1.125	483	23.5	98.35	2.64	8.2	10.9	13.3
-0.875	426	29.9	111.45	2.36	7.4	9.77	12.4
-0.625	376	36.7	126.29	2.11	6.7	8.79	11.5
-0.375	332	43.8	143.10	1.89	6.0	7.91	10.6
-0.125	293	51.2	162.16	1.69	5.4	7.09	9.74
0.125	258	58.6	183.75	1.51	4.8	6.33	8.83
0.375	228	66.2	208.21	1.33	4.3	5.61	7.94
0.625	201	73.9	235.94	1.17	3.8	4.93	7.06
0.875	178	81.6	267.35	1.02	3.3	4.29	6.21
1.125	157	89.4	302.95	0.88	2.8	3.68	5.37
1.375	138	97.2	343.29	0.74	2.4	3.11	4.58
1.625	122	105	389.00	0.62	1.9	2.57	3.82
1.875	108	113	440.79	0.51	1.6	2.08	3.11
2.125	95.1	121	499.48	0.40	1.2	1.63	2.46
2.375	83.9	128	565.99	0.31	0.93	1.24	1.88
2.625	74.0	136	641.35	0.23	0.67	0.903	1.38
2.875	65.3	144	726.74	0.17	0.46	0.630	0.971
3.125	57.7	152	823.50	0.12	0.30	0.419	0.650
3.375	50.9	160	933.15	0.08	0.19	0.266	0.415
3.625	44.9	167	1057.40	0.05	0.11	0.161	0.253
3.875	39.6	175	1198.19	0.03	$0.60 \times 10^{-1}$	$0.939 \times 10^{-1}$	0.149
4.125	35.0	183	1357.73	0.02	$0.32 \times 10^{-1}$	$0.535 \times 10^{-1}$	$0.852 \times 10^{-1}$
4.375	30.9	191	1538.51	0.01	$0.16 \times 10^{-1}$	$0.300 \times 10^{-1}$	$0.480 \times 10^{-1}$
4.625	27.2	199	1743.36	0.01	$0.80 \times 10^{-2}$	$0.165 \times 10^{-1}$	$0.267 \times 10^{-1}$
4.875	24.0	206	1975.48	0.01	$0.38 \times 10^{-2}$	$0.892 \times 10^{-2}$	$0.145 \times 10^{-1}$
5.125	21.2	214	2238.52	0.00	$0.18 \times 10^{-2}$	$0.459 \times 10^{-2}$	$0.749 \times 10^{-2}$

TABLE II. The effective photon flux  $f_{\text{Pb}}$  and  $f_{\text{incoh}}$ ,  $f_{\text{coh}}$  radiated in the case of  $J/\psi$  production at proton-nucleon collision energy  $\sqrt{s_{pN}} = 5.02$  TeV by the lead ion and by the proton beam.

$Y_{\text{lab}}$	$W_{\text{Pb}}$ (GeV)	$f_{\text{Pb}}$	$W_p$ (GeV)	$f_{\text{incoh}}$	$f_{\text{coh}}$	$f_{\text{incoh}} + f_{\text{coh}}$	$f_{\text{incoh}} + f_{\text{coh}}(R_A = 1)$
-5.125	2040	$0.102 \times 10^{-3}$	7.62	5.68	$0.18 \times 10^{-1}$	5.70	4.16
-4.875	1800	$0.145 \times 10^{-2}$	8.63	5.50	0.29	5.79	4.06
-4.625	1590	$0.121 \times 10^{-1}$	9.78	5.21	1.3	6.54	4.49
-4.375	1400	$0.662 \times 10^{-1}$	11.08	4.80	3.1	7.90	5.44
-4.125	1240	0.257	12.56	4.10	4.5	8.63	6.41
-3.875	1090	0.759	14.23	3.31	5.0	8.30	7.03
-3.625	964	1.81	16.12	2.55	4.6	7.17	7.21
-3.375	851	3.63	18.27	1.93	3.9	5.80	7.04
-3.125	751	6.38	20.70	1.46	3.1	4.58	6.65
-2.875	663	10.1	23.46	1.12	2.5	3.58	6.13
-2.625	585	14.7	26.58	0.87	1.9	2.80	5.56
-2.375	516	20.2	30.12	0.69	1.5	2.22	4.98
-2.125	455	26.2	34.13	0.56	1.2	1.78	4.42
-1.875	402	32.8	38.68	0.47	1.0	1.46	3.89
-1.625	355	39.8	43.83	0.39	0.82	1.21	3.40
-1.375	313	47.0	49.66	0.34	0.68	1.02	2.95
-1.125	276	54.4	56.27	0.29	0.57	0.860	2.54
-0.875	244	61.9	63.77	0.25	0.48	0.733	2.18
-0.625	215	69.5	72.26	0.22	0.40	0.626	1.85
-0.375	190	77.2	81.88	0.20	0.34	0.535	1.57
-0.125	168	84.9	92.78	0.17	0.28	0.456	1.32
0.125	148	92.7	105.13	0.15	0.24	0.389	1.11
0.375	130	100	119.13	0.13	0.20	0.330	0.922
0.625	115	108	134.99	0.12	0.16	0.279	0.764
0.875	102	116	152.97	0.10	0.13	0.235	0.630
1.125	89.7	124	173.34	0.09	0.11	0.197	0.517
1.375	79.1	132	196.42	0.08	$0.86 \times 10^{-1}$	0.164	0.423
1.625	69.8	139	222.57	0.07	$0.69 \times 10^{-1}$	0.136	0.344
1.875	61.6	147	252.20	0.06	$0.54 \times 10^{-1}$	0.112	0.279
2.125	54.4	155	285.78	0.05	$0.42 \times 10^{-1}$	$0.918 \times 10^{-1}$	0.225
2.375	48.0	163	323.83	0.04	$0.33 \times 10^{-1}$	$0.748 \times 10^{-1}$	0.181
2.625	42.4	170	366.95	0.04	$0.25 \times 10^{-1}$	$0.605 \times 10^{-1}$	0.145
2.875	37.4	178	415.81	0.03	$0.19 \times 10^{-1}$	$0.486 \times 10^{-1}$	0.115
3.125	33.0	186	471.18	0.02	$0.14 \times 10^{-1}$	$0.388 \times 10^{-1}$	$0.911 \times 10^{-1}$
3.375	29.1	194	533.91	0.02	$0.11 \times 10^{-1}$	$0.307 \times 10^{-1}$	$0.717 \times 10^{-1}$
3.625	25.7	202	605.00	0.02	$0.78 \times 10^{-2}$	$0.242 \times 10^{-1}$	$0.562 \times 10^{-1}$
3.875	22.7	209	685.56	0.01	$0.56 \times 10^{-2}$	$0.190 \times 10^{-1}$	$0.437 \times 10^{-1}$
4.125	20.0	217	776.84	0.01	$0.40 \times 10^{-2}$	$0.148 \times 10^{-1}$	$0.339 \times 10^{-1}$
4.375	17.7	225	880.27	0.01	$0.29 \times 10^{-2}$	$0.114 \times 10^{-1}$	$0.262 \times 10^{-1}$
4.625	15.6	233	997.48	0.01	$0.20 \times 10^{-2}$	$0.884 \times 10^{-2}$	$0.202 \times 10^{-1}$
4.875	13.8	240	1130.29	0.01	$0.14 \times 10^{-2}$	$0.673 \times 10^{-2}$	$0.154 \times 10^{-1}$
5.125	12.1	248	1280.79	0.00	$0.96 \times 10^{-3}$	$0.505 \times 10^{-2}$	$0.116 \times 10^{-1}$

TABLE III. The effective photon flux  $f_{\text{Pb}}$  and  $f_{\text{incoh}}, f_{\text{coh}}$  radiated in the case of  $\Upsilon$  production at proton-nucleon collision energy  $\sqrt{s_{pN}} = 8.16$  TeV by the lead ion and by the proton beam.

$Y_{\text{lab}}$	$W_{\text{Pb}}$ (GeV)	$f_{\text{Pb}}$	$W_p$ (GeV)	$f_{\text{incoh}}$	$f_{\text{coh}}$	$f_{\text{incoh}} + f_{\text{coh}}$	$f_{\text{incoh}} + f_{\text{coh}}(R_A = 1)$
-5.125	4550	$0.548 \times 10^{-8}$	16.97	7.14	$0.90 \times 10^{-11}$	7.14	7.52
-4.875	4010	$0.482 \times 10^{-6}$	19.23	7.70	$0.35 \times 10^{-5}$	7.70	7.27
-4.625	3540	$0.190 \times 10^{-4}$	21.79	8.07	$0.33 \times 10^{-2}$	8.07	7.02
-4.375	3130	$0.374 \times 10^{-3}$	24.69	8.22	0.15	8.37	6.88
-4.125	2760	$0.410 \times 10^{-2}$	27.98	8.22	1.2	9.47	7.49
-3.875	2430	$0.279 \times 10^{-1}$	31.70	8.11	4.2	12.3	9.51
-3.625	2150	0.129	35.92	7.85	8.4	16.3	12.4
-3.375	1900	0.437	40.70	7.37	12	19.5	15.2
-3.125	1670	1.16	46.12	6.65	14	20.8	17.2
-2.875	1480	2.54	52.26	5.92	15	20.7	18.3
-2.625	1300	4.78	59.22	5.23	14	19.5	18.7
-2.375	1150	7.99	67.11	4.61	13	18.0	18.5
-2.125	1010	12.2	76.04	4.08	12	16.4	18.0
-1.875	896	17.2	86.17	3.65	11	14.9	17.4
-1.625	790	23.0	97.64	3.28	10	13.6	16.6
-1.375	697	29.3	110.64	2.97	9.4	12.4	15.7
-1.125	615	36.1	125.38	2.69	8.6	11.3	14.8
-0.875	543	43.2	142.07	2.45	7.9	10.3	13.9
-0.625	479	50.5	160.99	2.23	7.2	9.43	12.9
-0.375	423	58.0	182.42	2.03	6.6	8.60	12.0
-0.125	373	65.6	206.71	1.84	6.0	7.82	11.1
0.125	329	73.2	234.23	1.67	5.4	7.07	10.1
0.375	291	80.9	265.42	1.50	4.9	6.37	9.21
0.625	257	88.7	300.76	1.34	4.4	5.69	8.31
0.875	226	96.5	340.81	1.19	3.9	5.04	7.43
1.125	200	104	386.19	1.04	3.4	4.42	6.57
1.375	176	112	437.61	0.91	2.9	3.83	5.73
1.625	156	120	495.87	0.78	2.5	3.27	4.93
1.875	137	128	561.90	0.65	2.1	2.75	4.17
2.125	121	135	636.72	0.54	1.7	2.26	3.45
2.375	107	143	721.49	0.44	1.4	1.81	2.79
2.625	94.4	151	817.56	0.35	1.1	1.41	2.19
2.875	83.3	159	926.42	0.27	0.79	1.06	1.66
3.125	73.5	167	1049.77	0.20	0.57	0.766	1.20
3.375	64.9	174	1189.54	0.14	0.39	0.530	0.837
3.625	57.2	182	1347.93	0.10	0.25	0.348	0.555
3.875	50.5	190	1527.40	0.07	0.15	0.219	0.351
4.125	44.6	198	1730.77	0.04	$0.87 \times 10^{-1}$	0.132	0.212
4.375	39.3	206	1961.22	0.03	$0.48 \times 10^{-1}$	$0.766 \times 10^{-1}$	0.124
4.625	34.7	213	2222.35	0.02	$0.25 \times 10^{-1}$	$0.435 \times 10^{-1}$	$0.710 \times 10^{-1}$
4.875	30.6	221	2518.26	0.01	$0.13 \times 10^{-1}$	$0.244 \times 10^{-1}$	$0.400 \times 10^{-1}$
5.125	27.0	229	2853.56	0.01	$0.62 \times 10^{-2}$	$0.135 \times 10^{-1}$	$0.222 \times 10^{-1}$

TABLE IV. The effective photon flux  $f_{\text{Pb}}$  and  $f_{\text{incoh}}, f_{\text{coh}}$  radiated in the case of  $J/\psi$  production at proton-nucleon collision energy  $\sqrt{s_{pN}} = 8.16$  TeV by the lead ion and by the proton beam.

$Y_{\text{lab}}$	$W_{\text{Pb}}$ (GeV)	$f_{\text{Pb}}$	$W_p$ (GeV)	$f_{\text{incoh}}$	$f_{\text{coh}}$	$f_{\text{incoh}} + f_{\text{coh}}$	$f_{\text{incoh}} + f_{\text{coh}}(R_A = 1)$
-5.125	2600	$0.102 \times 10^{-1}$	9.71	5.80	1.4	7.19	4.94
-4.875	2300	$0.577 \times 10^{-1}$	11.00	5.37	3.3	8.70	5.99
-4.625	2030	0.230	12.47	4.63	5.0	9.62	7.11
-4.375	1790	0.695	14.13	3.76	5.6	9.36	7.86
-4.125	1580	1.68	16.01	2.91	5.2	8.15	8.11
-3.875	1390	3.43	18.14	2.21	4.4	6.64	7.97
-3.625	1230	6.10	20.55	1.68	3.6	5.27	7.56
-3.375	1080	9.73	23.29	1.30	2.8	4.13	7.01
-3.125	957	14.3	26.39	1.01	2.2	3.25	6.39
-2.875	845	19.7	29.90	0.80	1.8	2.57	5.76
-2.625	746	25.7	33.89	0.66	1.4	2.09	5.14
-2.375	658	32.2	38.40	0.55	1.2	1.72	4.55
-2.125	581	39.2	43.51	0.46	0.97	1.43	4.00
-1.875	512	46.4	49.30	0.40	0.81	1.21	3.49
-1.625	452	53.7	55.87	0.34	0.68	1.03	3.03
-1.375	399	61.3	63.31	0.30	0.58	0.880	2.62
-1.125	352	68.9	71.74	0.27	0.49	0.758	2.25
-0.875	311	76.6	81.29	0.24	0.42	0.653	1.92
-0.625	274	84.3	92.11	0.21	0.35	0.562	1.63
-0.375	242	92.0	104.37	0.19	0.30	0.484	1.38
-0.125	214	99.8	118.27	0.17	0.25	0.415	1.16
0.125	188	108	134.02	0.15	0.21	0.356	0.974
0.375	166	115	151.86	0.13	0.17	0.303	0.814
0.625	147	123	172.08	0.12	0.14	0.258	0.678
0.875	130	131	195.00	0.10	0.12	0.218	0.564
1.125	114	139	220.96	0.09	$0.95 \times 10^{-1}$	0.184	0.467
1.375	101	146	250.38	0.08	$0.77 \times 10^{-1}$	0.155	0.387
1.625	89.0	154	283.72	0.07	$0.62 \times 10^{-1}$	0.130	0.319
1.875	78.6	162	321.50	0.06	$0.49 \times 10^{-1}$	0.109	0.263
2.125	69.3	170	364.30	0.05	$0.39 \times 10^{-1}$	$0.904 \times 10^{-1}$	0.217
2.375	61.2	178	412.81	0.04	$0.31 \times 10^{-1}$	$0.750 \times 10^{-1}$	0.178
2.625	54.0	185	467.77	0.04	$0.24 \times 10^{-1}$	$0.619 \times 10^{-1}$	0.145
2.875	47.7	193	530.06	0.03	$0.19 \times 10^{-1}$	$0.508 \times 10^{-1}$	0.119
3.125	42.1	201	600.63	0.03	$0.14 \times 10^{-1}$	$0.416 \times 10^{-1}$	$0.963 \times 10^{-1}$
3.375	37.1	209	680.61	0.02	$0.11 \times 10^{-1}$	$0.338 \times 10^{-1}$	$0.778 \times 10^{-1}$
3.625	32.8	216	771.23	0.02	$0.83 \times 10^{-2}$	$0.273 \times 10^{-1}$	$0.627 \times 10^{-1}$
3.875	28.9	224	873.92	0.02	$0.62 \times 10^{-2}$	$0.219 \times 10^{-1}$	$0.501 \times 10^{-1}$
4.125	25.5	232	990.28	0.01	$0.46 \times 10^{-2}$	$0.174 \times 10^{-1}$	$0.398 \times 10^{-1}$
4.375	22.5	240	1122.13	0.01	$0.33 \times 10^{-2}$	$0.138 \times 10^{-1}$	$0.315 \times 10^{-1}$
4.625	19.9	248	1271.54	0.01	$0.24 \times 10^{-2}$	$0.108 \times 10^{-1}$	$0.248 \times 10^{-1}$
4.875	17.5	255	1440.85	0.01	$0.17 \times 10^{-2}$	$0.852 \times 10^{-2}$	$0.195 \times 10^{-1}$
5.125	15.5	263	1632.69	0.01	$0.12 \times 10^{-2}$	$0.663 \times 10^{-2}$	$0.152 \times 10^{-1}$

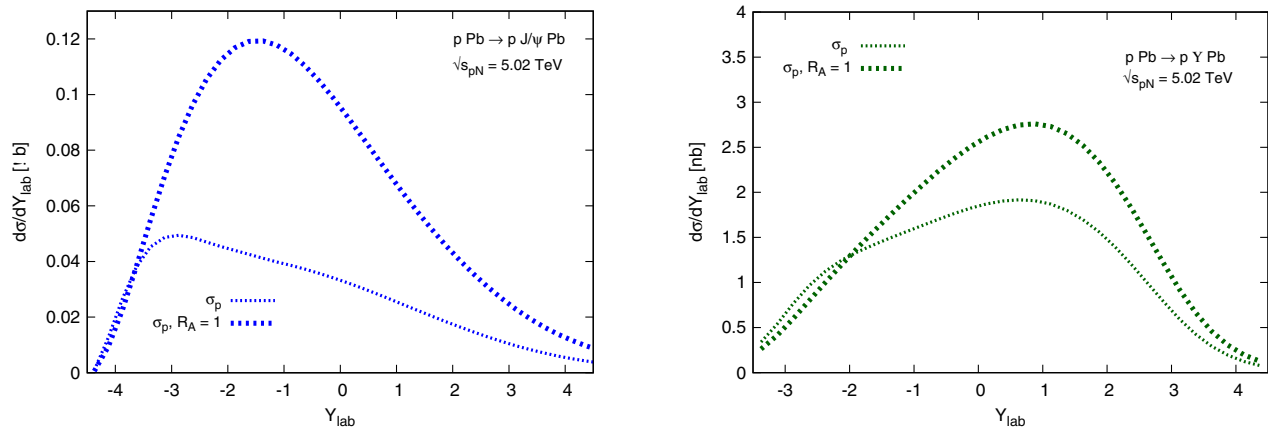


FIG. 8. The contribution due to the term where the photon is emitted from the proton,  $\sigma_p$ , with and without inclusion of the nuclear modification factor  $R_A$ . The left panel is for the  $J/\psi$  production at  $\sqrt{s_{pN}} = 5.02$  TeV and the right panel is for  $\Upsilon$  production at the same center-of-mass energy.

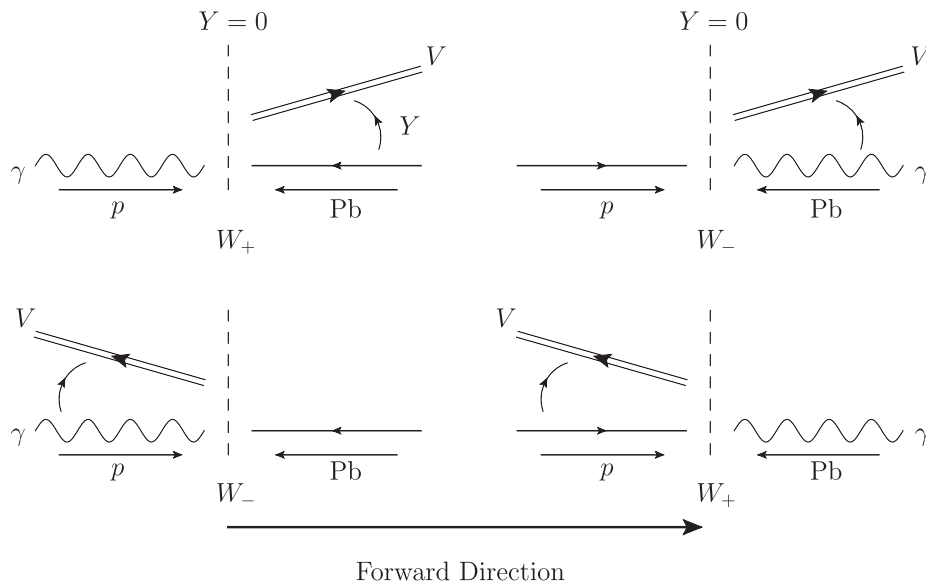


FIG. 9. The four kinematic configurations for exclusive heavy vector meson  $V$  ultraperipheral production in  $p$ -Pb collisions at a given rapidity  $Y$  occurring via a photoproduction subprocess at two energies,  $W_+$  and  $W_-$ . The incoming photon is a Weizsäcker-Williams photon that has been emitted from a proton (lead nucleus) and interacts with an incoming lead nucleus (proton). The vector meson can travel in the direction of the photon ( $W_+$ ) or against the direction of the photon ( $W_-$ ).

- [1] D. Yu. Ivanov, A. Schafer, L. Szymanowski, and G. Krasnikov, Exclusive photoproduction of a heavy vector meson in QCD, *Eur. Phys. J. C* **34**, 297 (2004); Erratum, *Eur. Phys. J. C* **75**, 75 (2015).
- [2] S. P. Jones, A. D. Martin, M. G. Ryskin, and T. Teubner, The exclusive  $J/\psi$  process at the LHC tamed to probe the low  $x$  gluon, *Eur. Phys. J. C* **76**, 633 (2016).

- [3] E. Iancu, K. Itakura, and S. Munier, Saturation and BFKL dynamics in the HERA data at small  $x$ , *Phys. Lett. B* **590**, 199 (2004).
- [4] H. Kowalski, L. Motyka, and G. Watt, Exclusive diffractive processes at HERA within the dipole picture, *Phys. Rev. D* **74**, 074016 (2006).

- [5] S. P. Jones, A. D. Martin, M. G. Ryskin, and T. Teubner, Exclusive  $J/\psi$  production at the LHC in the  $k_T$  factorization approach, *J. Phys. G* **44**, 03LT01 (2017).
- [6] V. Guzey and M. Zhalov, Rapidity and momentum transfer distributions of coherent  $J/\psi$  photoproduction in ultra-peripheral  $p$ Pb collisions at the LHC, *J. High Energy Phys.* **02** (2014) 046.
- [7] A. G. Shuvaev, K. J. Golec-Biernat, A. D. Martin, and M. G. Ryskin, Off diagonal distributions fixed by diagonal partons at small  $x$  and  $\xi$ , *Phys. Rev. D* **60**, 014015 (1999).
- [8] A. Shuvaev, Solution of the off forward leading logarithmic evolution equation based on the Gegenbauer moments inversion, *Phys. Rev. D* **60**, 116005 (1999).
- [9] S. Bailey, T. Cridge, L. A. Harland-Lang, A. D. Martin, and R. S. Thorne, Parton distributions from LHC, HERA, Tevatron and fixed target data: MSHT20 PDFs, *Eur. Phys. J. C* **81**, 341 (2021).
- [10] C. A. Flett, S. P. Jones, A. D. Martin, M. G. Ryskin, and T. Teubner, How to include exclusive  $J/\psi$  production data in global PDF analyses, *Phys. Rev. D* **101**, 094011 (2020).
- [11] R. Aaij *et al.*, Updated measurements of exclusive  $J/\psi$  and  $\psi(2S)$  production cross-sections in pp collisions at  $\sqrt{s} = 7$  TeV, *J. Phys. G* **41**, 055002 (2014).
- [12] R. Aaij *et al.*, Central exclusive production of  $J/\psi$  and  $\psi(2S)$  mesons in  $pp$  collisions at  $\sqrt{s} = 13$  TeV, *J. High Energy Phys.* **10** (2018) 167.
- [13] C. A. Flett, S. P. Jones, A. D. Martin, M. G. Ryskin, and T. Teubner, Predictions of exclusive  $\Upsilon$  photoproduction at the LHC and future colliders, *Phys. Rev. D* **105**, 034008 (2022).
- [14] V. M. Budnev, I. F. Ginzburg, G. V. Meledin, and V. G. Serbo, The Two photon particle production mechanism. Physical problems, Applications. Equivalent photon approximation, *Phys. Rep.* **15**, 181 (1975).
- [15] V. A. Khoze, A. D. Martin, and M. G. Ryskin, Multiple interactions and rapidity gap survival, *J. Phys. G* **45**, 053002 (2018).
- [16] L. A. Harland-Lang, V. A. Khoze, A. D. Martin, and M. G. Ryskin, Searching for the odderon in ultraperipheral proton-ion collisions at the LHC, *Phys. Rev. D* **99**, 034011 (2019).
- [17] L. A. Harland-Lang, V. A. Khoze, and M. G. Ryskin, Exclusive LHC physics with heavy ions: SuperChic 3, *Eur. Phys. J. C* **79**, 39 (2019).
- [18] M. Vidovic, M. Greiner, C. Best, and G. Soff, Impact parameter dependence of the electromagnetic particle production in ultrarelativistic heavy ion collisions, *Phys. Rev. C* **47**, 2308 (1993).
- [19] J. J. Sakurai, Theory of strong interactions, *Ann. Phys. (N.Y.)* **11**, 1 (1960).
- [20] T. H. Bauer, R. D. Spital, D. R. Yennie, and F. M. Pipkin, The hadronic properties of the photon in high-energy interactions, *Rev. Mod. Phys.* **50**, 261 (1978); Erratum, *Rev. Mod. Phys.* **51**, 407 (1979).
- [21] V. A. Khoze, A. D. Martin, and M. G. Ryskin, Exclusive vector meson production in heavy ion collisions, *J. Phys. G* **46**, 085002 (2019).
- [22] B. Z. Kopeliovich, L. I. Lapidus, and A. B. Zamolodchikov, Dynamics of color in hadron diffraction on nuclei, *JETP Lett.* **33**, 595 (1981).
- [23] G. Bertsch, S. J. Brodsky, A. S. Goldhaber, and J. F. Gunion, Diffractive Excitation in QCD, *Phys. Rev. Lett.* **47**, 297 (1981).
- [24] B. Alessandro *et al.*,  $J/\psi$  and  $\psi'$  production and their normal nuclear absorption in proton-nucleus collisions at 400 GeV, *Eur. Phys. J. C* **48**, 329 (2006).
- [25] V. S. Fadin and L. N. Lipatov, BFKL pomeron in the next-to-leading approximation, *Phys. Lett. B* **429**, 127 (1998).
- [26] M. Ciafaloni and G. Camici, Energy scale(s) and next-to-leading BFKL equation, *Phys. Lett. B* **430**, 349 (1998).
- [27] G. P. Salam, A resummation of large subleading corrections at small  $x$ , *J. High Energy Phys.* **07** (1998) 019.
- [28] M. Ciafaloni and D. Colferai, The BFKL equation at next-to-leading level and beyond, *Phys. Lett. B* **452**, 372 (1999).
- [29] G. Antchev *et al.*, Measurement of elastic  $pp$  scattering at  $\sqrt{s} = 8$  TeV in the Coulomb-nuclear interference region: Determination of the  $\rho$ -parameter and the total cross-section, *Eur. Phys. J. C* **76**, 661 (2016).
- [30] H. Stenzel, Measurement of the total cross section at 8 TeV and the inelastic cross section at 13 TeV at the LHC with the ATLAS detector, *AIP Conf. Proc.* **1819**, 040005 (2017).
- [31] K. J. Eskola, P. Paakkinen, H. Paukkunen, and C. A. Salgado, EPPS16: Nuclear parton distributions with LHC data, *Eur. Phys. J. C* **77**, 163 (2017).
- [32] B. B. Abelev *et al.*, Exclusive  $J/\psi$  Photoproduction off Protons in Ultra-Peripheral  $p$ Pb Collisions at  $\sqrt{s_{NN}} = 5.02$  TeV, *Phys. Rev. Lett.* **113**, 232504 (2014).
- [33] S. Acharya *et al.*, Energy dependence of exclusive  $J/\psi$  photoproduction off protons in ultra-peripheral  $p$ Pb collisions at  $\sqrt{s_{NN}} = 5.02$  TeV, *Eur. Phys. J. C* **79**, 402 (2019).
- [34] A. M. Sirunyan *et al.*, Measurement of exclusive  $\Upsilon$  photoproduction from protons in  $p$ Pb collisions at  $\sqrt{s_{NN}} = 5.02$  TeV, *Eur. Phys. J. C* **79**, 277 (2019).
- [35] C. A. Flett, A. D. Martin, M. G. Ryskin, and T. Teubner, Very low  $x$  gluon density determined by LHCb exclusive  $J/\psi$  data, *Phys. Rev. D* **102**, 114021 (2020).
- [36] Zi-Qiang Chen and Cong-Feng Qiao, NLO QCD corrections to exclusive electroproduction of quarkonium, *Phys. Lett. B* **797**, 134816 (2019); Erratum, *Phys. Lett. B* **135759** (2020).
- [37] C. A. Flett, J. A. Gracey, S. P. Jones, and T. Teubner, Exclusive heavy vector meson electroproduction to NLO in collinear factorisation, *J. High Energy Phys.* **08** (2021) 150.
- [38] G. T. Bodwin, E. Braaten, and G. P. Lepage, Rigorous QCD analysis of inclusive annihilation and production of heavy quarkonium, *Phys. Rev. D* **51**, 1125 (1995); Erratum, *Phys. Rev. D* **55**, 5853 (1997).
- [39] S. P. Jones, A. D. Martin, M. G. Ryskin, and T. Teubner, Exclusive  $J/\psi$  and  $\Upsilon$  photoproduction and the low  $x$  gluon, *J. Phys. G* **43**, 035002 (2016).
- [40] M. G. Ryskin, R. G. Roberts, A. D. Martin, and E. M. Levin, Diffractive  $J/\psi$  photoproduction as a probe of the gluon density, *Z. Phys. C* **76**, 231 (1997).
- [41] C. Adloff *et al.*, Diffractive photoproduction of  $\psi(2S)$  mesons at HERA, *Phys. Lett. B* **541**, 251 (2002).
- [42] V. A. Khoze, A. D. Martin, and M. G. Ryskin, Diffraction at the LHC, *Eur. Phys. J. C* **73**, 2503 (2013).

- [43] D. Dutta, K. Naskar, R. Chudasama, and P. Sarin, Study of Upsilon photoproduction in  $p$ Pb collisions at 8.16 TeV with CMS experiment, DAE Symp. Nucl. Phys. **62**, 964 (2017).
- [44] K. Naskar, D. Dutta, and P. Sarin, Background study of Upsilon photoproduction in  $p$ Pb collisions at 8.16 TeV with CMS experiment, DAE Symp. Nucl. Phys. **63**, 958 (2018).
- [45] R. D. Woods and D. S. Saxon, Diffuse surface optical model for nucleon-nuclei scattering, *Phys. Rev.* **95**, 577 (1954).
- [46] C. M. Tarbert *et al.*, Neutron Skin of  $^{208}\text{Pb}$  from Coherent Pion Photoproduction, *Phys. Rev. Lett.* **112**, 242502 (2014).
- [47] A. B. Jones and B. A. Brown, Two-parameter Fermi function fits to experimental charge and point-proton densities for  $^{208}\text{Pb}$ , *Phys. Rev. C* **90**, 067304 (2014).
- [48] K. J. Eskola, C. A. Flett, V. Guzey, T. Löytäinen, and H. Paukkunen, Exclusive  $J/\psi$  photoproduction in ultraperipheral Pb + Pb collisions at the CERN Large Hadron Collider calculated at next-to-leading order perturbative QCD, *Phys. Rev. C* **106**, 035202 (2022).